Carbohydrate Polymers 337 (2024) 122170

Contents lists available at ScienceDirect

Carbohydrate Polymers

journal homepage: www.elsevier.com/locate/carbpol

Glyoxal crosslinking of electro-responsive alginate-based hydrogels: Effects on the properties

Samuele Colombi [a,b], Isabel Sáez [a], Nuria Borras [a], Francesc Estrany [a,b], Maria M. Pérez-Madrigal [a,b], José García-Torres [b,c,*], Jorge Morgado [d,**], Carlos Alemán [a,b,e,***]

[a] IMEM-BRT Group, Departament d'Enginyeria Química, EEBE, Universitat Politècnica de Catalunya - BarcelonaTech, C/ Eduard Maristany 10-14, 08019 Barcelona, Spain

[b] Barcelona Research Center in Multiscale Science and Engineering, Universitat Politècnica de Catalunya – BarcelonaTech, C/ Eduard Maristany 10-14, 08019 Barcelona, Spain

[c] Biomaterials, Biomechanics and Tissue Engineering Group, Department of Materials Science and Engineering, Universitat Politècnica de Catalunya – BarcelonaTech, C/ Eduard Maristany 10-14, 08019 Barcelona, Spain

[d] Department of Bioengineering, Instituto de Telecomunicações, Instituto Superior Técnico, Universidade de Lisboa, Av. Rovisco Pais, 1049-001 Lisboa, Portugal

[e] Institute for Bioengineering of Catalonia (IBEC), The Barcelona Institute of Science and Technology, Baldiri Reixac 10-12, 08028 Barcelona, Spain

ARTICLE INFO

Keywords:
Conducting hydrogels
Semi-interpenetrated hydrogel
Poly(3,4-ethylenedioxythiophene)
Electrochemical biosensor
Dual network

ABSTRACT

To improve the features of alginate-based hydrogels in physiological conditions, Ca^{2+}-crosslinked semi-interpenetrated hydrogels formed by poly(3,4-ethylenedioxythiophene):polystyrene sulfonic acid and alginate (PEDOT/Alg) were subjected to a treatment with glyoxal to form a dual ionic/covalent network. The covalent network density was systematically varied by considering different glyoxalization times (t_G). The content of Ca^{2+} was significantly higher for the untreated hydrogel than for the glyoxalized ones, while the properties of the hydrogels were found to largely depend on t_G. The porosity and swelling capacity decreased with increasing t_G, while the stiffness and electrical conductance retention capacity increased with t_G. The potentiodynamic response of the hydrogels notably depended on the amount of conformational restraints introduced by the glyoxal, which is a very short crosslinker. Thus, the re-accommodation of the polymer chains during the cyclic potential scans became more difficult with increasing number of covalent crosslinks. This information was used to improve the performance of untreated PEDOT/Alg as electrochemical sensor of hydrogen peroxide by simply applying a t_G of 5 min. Overall, the control of the properties of glyoxalized hydrogels through t_G is very advantageous and can be used as an on-demand strategy to improve the performance of such materials depending on the application.

1. Introduction

Alginate (Alg), which is a naturally occurring water-soluble polysaccharide typically obtained from brown-algae cell walls, has been extensively investigated and used for many biomedical applications, due to its biocompatibility, low toxicity, relatively low cost, and easy gelation under mild conditions by adding divalent cations (Grijalvo, Nieto-Díaz, Maza, Eritja, & Díaz, 2019; Wang et al., 2023; Yang et al., 2022). In addition, Alg is also widely used in other areas, like pharmacy, chemical engineering, agriculture, and food industry (Guo, Wang, Qin, Shen, & Peng, 2020; Klein & Poverenov, 2020; Manzoor et al., 2022). This anionic polymer, which is composed of irregular blocks of β-D-mannuronic acid (M) and 1–4 linked α-L-guluronic residues (G), forms hydrogels when divalent cations ionically crosslink the G-blocks of polymer chains through the so-called "egg-box" structure (*i.e.* the M blocks form weak ionic bonds with divalent cations) (Braccini & Pérez, 2001; Grant, Morris, Rees, Smith, & Thom, 1973; Solberg, Draget, Schatz, & Christensen, 2023). The substitution of divalent cations by

* Correspondence to: J. García-Torres, Barcelona Research Center in Multiscale Science and Engineering, Universitat Politècnica de Catalunya – BarcelonaTech, C/ Eduard Maristany 10-14, 08019 Barcelona, Spain.

** Corresponding author.

*** Correspondence to: C. Alemán, IMEM-BRT Group, Departament d'Enginyeria Química, EEBE, Universitat Politècnica de Catalunya - BarcelonaTech, C/ Eduard Maristany 10-14, 08019 Barcelona, Spain.

E-mail addresses: jose.manuel.garcia-torres@upc.edu (J. García-Torres), jmfmorgado@tecnico.ulisboa.pt (J. Morgado), carlos.aleman@upc.edu (C. Alemán).

https://doi.org/10.1016/j.carbpol.2024.122170
Received 2 January 2024; Received in revised form 8 April 2024; Accepted 14 April 2024
Available online 15 April 2024

monovalent cations, such as Na^+, causes the disruption of the hydrogel network, which can be an advantage or a disadvantage depending on the final application (Bajpai & Sharma, 2004; Ionita, Ariciu, Smith, & Chechik, 2015; LeRoux, Guilak, & Setton, 1999; Li, Srebnik, & Rojas, 2022; Pérez-Madrigal et al., 2017). For example, ionic bonds in divalent cation-crosslinked Alg hydrogels might be dissociated in physiological environments leading to inhomogeneous weak structures through an ion exchange process, which limits their utilization in structural biomedical applications but facilitates their use as drug delivery systems (Bajpai & Sharma, 2004; Ionita et al., 2015). Also, cell viability and proliferation are significantly affected by such divalent cations (Cao, Chen, & Schreyer, 2012).

In recent years, Alg-based hydrogels with electrical conductivity and electrochemical responsiveness have been developed by incorporating conductive materials. Although such materials can be obtained by simple immobilization of conductive nanomaterials (*e.g.* graphene and carbon nanotubes) (Alabi, Aubry, & Zou, 2022; Joddar, Garcia, Casas, & Stewart, 2016; Luu et al., 2022; Mottet et al., 2018), the most effective procedure is the formation of semi-interpenetrated hydrogel networks with conducting polymers (CPs) (García-Torres, Colombi, Macor, & Alemán, 2022; Ji et al., 2022). Semi-interpenetrated CP/Alg hydrogels have been successfully used to develop sensors (Babeli et al., 2020; Babeli et al., 2021; Ren et al., 2019), drug delivery systems (Bogdanova et al., 2022; Kaklamani et al., 2018; Puiggalí-Jou et al., 2020), and soft electronic devices (Da Silva, Wang, & Minev, 2022; Puiggalí-Jou et al., 2021; Yang et al., 2016), among others. Nevertheless, semi-interpenetrated CP/Alg hydrogels in which polysaccharide chains are only ionically crosslinked through divalent cations experience the same limitation as the neat Alg hydrogels when in presence of monovalent cations (Babeli et al., 2020; Babeli et al., 2021; Bogdanova et al., 2022; Da Silva et al., 2022; García-Torres et al., 2022; Ji et al., 2022; Kaklamani et al., 2018; Puiggalí-Jou et al., 2020; Puiggalí-Jou et al., 2021; Ren et al., 2019; Yang et al., 2016).

A wide variety of crosslinkers with different functionalities has been used to covalently crosslink Alg chains for hydrogel formation, as for example diamino-terminated polyethylene glycol (PEG) (Eiselt, Lee, & Mooney, 1999), polyethyleneimine (PEI) (Rajaram, Schreyer, & Chen, 2015; Zhang et al., 2018), adipic acid dihydrazide (Wang, Shansky, Borselli, Mooney, & Vandenburgh, 2012), disulfide tetrazine (Siboro et al., 2021), and acrylamide (Pragya et al., 2021). Thus, the combination of ionic and covalent crosslinks in the network contributes to preserve the stability of Alg hydrogels in environments without divalent cations, as well as, in general, improves their properties (Feyissa, Edossa, Gupta, & Negera, 2023; Meng et al., 2014; Samorezov, Morlock, & Alsberg, 2015; Szabó et al., 2019). Besides, although their performance could be further enhanced by exploiting functionalized crosslinkers, these elements have never been used to form CP/Alg hydrogels with dual ionic/covalent networks.

Glyoxal, a dialdehyde with relatively low toxicity that is obtained from renewable resources and shows partial biodegradability (Miyata, Kurokawa, & De Strihou, 2000; Ramires, Megiatto Jr., Gardrat, Castellan, & Frollini, 2010; Rojas & Azevedo, 2011), has been used as crosslinking agent for chitosan (Chen, Monnier, Gällstedt, Gedde, & Hedenqvist, 2014; Elsayed, Monier, Alatawi, Albalawi, & Alhawiti, 2022; Kumar & Kumar, 2017), cellulose (Castro et al., 2015; Kumar & Kumar, 2017; Quero et al., 2011), and polyvinyl alcohol (Dey, Bera, Bera, & Chakrabart, 2014; Kumar & Kumar, 2017; Panigrahi, Kumar, & Dhar, 2019). Nevertheless, no application of glyoxal has, to the best of our knowledge, been proposed to crosslink Alg-based hydrogels. In this work, we covalently crosslink Alg polymer chains in a semi-interpenetrated CP/Alg hydrogel using a simple glyoxalization process. More specifically, the CP selected for this purpose is poly(3,4-ethylenedioxythiophene):polystyrene sulfonic acid (PEDOT:PSS), which is easy to handle, water-soluble, biocompatible, and exhibits high electrical conductivity and stable electrochemical properties (Du, Yang, & Liu, 2023; He et al., 2019; Wang & Liu, 2023). PEDOT/Alg hydrogels, which are rapidly formed by replacing PSS chains with Alg chains when Alg is mixed with PEDOT:PSS and $CaCl_2$ is added, have been proposed for sensors (Babeli et al., 2020; Babeli et al., 2021) and soft electronics (Puiggalí-Jou et al., 2021). Despite such enormous potential, PEDOT/Alg hydrogels tend to disassemble and their mechanical properties decrease when are exposed to Ca^{2+}-free solutions, which limits their practical application.

In this work, we hypothesize that glyoxal can be successfully used to covalently crosslink Alg chains in semi-interpenetrated PEDOT/Alg hydrogels, improving its properties and stability. For this purpose, PEDOT/Alg hydrogels have been prepared using different glyoxalization times (t_G = 5, 15, 30, 60 and 120 min). After characterizing the properties and the dual crosslinking network, glyoxalized hydrogels have been used as electrochemical biosensors for the detection of hydrogen peroxide (H_2O_2). Overall, in this work we show that, in general, the properties of glyoxalized PEDOT/Alg can be regulated through t_G, opening an advantageous *a la carte* strategy to improve the performance of PEDOT/Alg hydrogels for each application.

2. Methods

2.1. Materials

Alginic acid (AA) from *Macrocystis pyrifera* (61 % mannuronic acid and 39 % guluronic acid; M_W = 240 kDa; commercial grade) was purchased from Sigma-Aldrich, while $CaCl_2$ (≥99.0 %) was purchased from Scharlab. Clevios™ PH 1000 commercial grade PEDOT:PSS (hereafter PEDOT:PSS), which, according to the manufactures, exhibits a conductivity of 1000 S/cm, was purchased from Heraeus Epurio as a water dispersion (1.3 wt%).

Commercial grade glyoxal, as a water dispersion (40 wt%), aluminum sulfate octadecahydrate ($Al_2(SO_4)_3{\cdot}18H_2O$; 99.99 %), phosphate buffered saline (PBS), ethyl acetate (HPLC grade), hydrogen peroxide solution (% Purity, titration: 29.0–32.0), and calconcarboxylic acid (Patton and Reeder (PR) indicator) were purchased from Sigma-Aldrich. Acetone (≥ 99.0 %) and isopropanol (Reagent grade) were purchased from Honeywell.

2.2. Preparation of PEDOT/Alg hydrogel

PEDOT/Alg hydrogel was prepared using a previously described procedure (Babeli et al., 2020). In brief, a 1.3 wt% AA solution was prepared by dissolving the biopolymer in deionized water (pH 6.7) at 50 °C with vigorous stirring for 1 h. Despite temperature and stirring, it was not possible to obtain a completely transparent and clear AA solution but a translucent and viscous solution, suggesting that AA was swollen rather than dissolved. Then, a 1:1 PEDOT:PSS/AA mixture was prepared mixing at room temperature equal volumes of the 1.3 wt% PEDOT:PSS dispersion and the 1.3 wt% AA solution. The mixture was kept under vigorous stirring for 20 min. PEDOT/Alg hydrogel was formed by immersing silicon rubber molds filled with 3 mL (5.0 × 3.0 × 0.3 cm^3 molds) of the 1:1 PEDOT:PSS/AA mixture into a $CaCl_2$ 3 wt% aqueous solution for 10 min (Babeli et al., 2020). It is worth mentioning that the molds were used to control the dimensions of the hydrogel for reproducibility. Finally, blotting paper was used to remove excess water from the surface of the hydrogels and thus prevent water leaking during measurements. The preparation of PEDOT/Alg hydrogels was replicated several times ($n > 10$) for characterization assays.

2.3. Glyoxal treatment of PEDOT/Alg hydrogel

Hydrogel samples were immersed in 2 mL of an aqueous solution at 50 °C containing glyoxal (5 wt%) and $Al_2(SO_4)_3$ (1 g/L), which catalyzed the glyoxalization reaction. Hydrogels were kept in the glyoxal/$Al_2(SO_4)_3$ solution for different times (t_G): 5 min (PEDOT/Alg/G5), 15 min (PEDOT/Alg/G15), 30 min (PEDOT/Alg/G30), 60 min (PEDOT/

ALG/G60) or 120 min (PEDOT/ALG/G120). After the corresponding t_G, samples were washed in deionized water at 70 °C for 60 min to remove the excess of glyoxal. It should be mentioned that, in order to avoid the loss of Ca^{2+} ions and preserve their stability, said washing step was not applied to the untreated PEDOT/Alg (control) hydrogels. The preparation of glyoxalized PEDOT/Alg hydrogels was replicated several times ($n > 10$) for characterization assays.

2.4. Characterization

FTIR absorption spectra of lyophilized hydrogels were recorded on a FTIR Jasco 4100 spectrophotometer. Samples were placed in an attenuated total reflection accessory (Top-plate) with a diamond crystal (Specac model MKII Golden Gate Heated Single Reflection Diamond ATR). For each sample, 64 scans were performed between 4000 and 600 cm^{-1} with a resolution of 4 cm^{-1}. For the sake of comparison, all the *spectra* were *normalized with respect* of the absorption band at 1622 cm^{-1}, which was the most intense for PEDOT/Alg.

Untreated and glyoxalized Alg hydrogels (*i.e.* without semi-interpenetrating PEDOT) were analyzed by ^{1}H NMR and ^{13}C NMR spectroscopy. All NMR spectra were acquired with a Bruker Avance III-400 spectrometer operating at 400.1 MHz.

In ^{1}H NMR spectra, the chemical shift was calibrated using tetramethylsilane as internal standard. Sixty-four scans were recorded in all cases. The spectrum of untreated Alg was obtained after dissolving 12.3 mg of AA in 550 μL of deuterated water by applying sonication for 24 h at 37 °C. Glyoxalized Alg hydrogel was obtained using $t_G = 30$ min. The formed hydrogel (100 mg) was lyophilized and finely grounded with a mortar and, subsequently, 14.4 mg of the resulting powder were dispersed in 550 μL of deuterated water by applying sonication for 24 h at 37 °C. For each studied hydrogel, two spectra were acquired using independent samples ($n = 2$).

For solid state ^{13}C NMR spectra, lyophilized Ca^{2+}-crosslinked Alg and glyoxalized Alg were grinded and transferred into 4 mm Bruker-style zirconia MAS rotors as dry powders. Spectra were recorded using cross-polarization magic angle spinning, applying a spin rate of 10,000 rpm.

Scanning electron microscopy (SEM) studies were performed to examine the morphology of control and glyoxalized hydrogels (micrographs were taken using three independent samples, $n = 3$, for each studied hydrogel). Lyophilized (*i.e.* freeze-drying) samples were placed in a Focussed Ion Beam Zeis Neon 40 scanning electron microscope operating at 5 kV, equipped with an energy dispersive X-ray (EDX) spectroscopy system. All samples were sputter-coated with a thin carbon layer using a K950X Turbo Evaporator to prevent electron charging problems.

The swelling ratios (*SR*, %) of the hydrogels in both 0.01 M phosphate buffered saline (PBS) solution (pH 7.3 and room temperature (RT)) and 3 wt% $CaCl_2$ aqueous solution ($n = 3$ for each medium) were evaluated using the following Eqn:

$$SR = \frac{w_W - w_D}{w_D} \quad (1)$$

where w_W is the weight of the hydrogels as prepared (after the washing step) and w_D is the weight of the hydrogel after freeze-drying (dried hydrogel). Swelling ratio evolution with time was monitored for 3 days.

The surface free energy (SFE) was determined using the Owens, Wendt, Rabel and Kaelble (OWRK) method using the contact angle with water and glycerol. Contact angle measurements were conducted using the sessile water drop method at room temperature and controlled humidity. Measurements were carried with the equipment OCA 20 (DataPhysics Instruments GmbH, Filderstadt), and the software SCA20 was used to analyze the data acquired ($n > 10$).

Quantitative nano-mechanical atomic force microscopy (AFM) mapping of the prepared hydrogels ($n = 9$) was performed using an AFM Dimension microscope using a NanoScope IV controller under ambient conditions in tapping mode. Measurements were done under ambient conditions and cantilevers were carefully calibrated. Quantitative nanomechanical allows quantitative evaluation of the material properties, including mechanical modulus. The proper probe was chosen depending on the expected Young's modulus (E) value of the sample. However, as the real E value is unknown before testing the sample, the probe is tentatively selected, as every kind of probe can cover a fairly large range of E values. TAP 150-G probes (Budget Sensors, Bulgaria) with a frequency of 150 kHz and a force constant of 5 N/m were used. The line scan rate was equal to 0.5–1.0 Hz.

2.5. Determination of calcium ion concentration

The content of Ca^{2+} in the hydrogels ($n = 3$) was analyzed using UV–Vis spectroscopy. For this purpose, hydrogels were immersed in 1 mL of PBS (incubation medium). To quantify the amount of Ca^{2+} ions released from the hydrogel, the incubation medium was removed and replaced by a fresh one after 1 h (0 days) and after 1 and 7 days. The removed medium was then centrifuged at 3000 rpm for 30 min and its UV–Vis spectrum was collected after addition of the PR indicator, while the Ca^{2+} content was quantified using calibration plots previously obtained with known Ca^{2+} concentrations (Fig. S1).

We observed that the incubation medium became cloudy when in contact with the prepared hydrogels, which was attributed to the release of aggregates formed by Alg chains that were insufficiently crosslinked. Those aggregates were probably stabilized by Ca^{2+} ions that would not have been quantified when performing the UV–Vis spectrum of the incubation medium. In order to quantify the Ca^{2+} trapped inside the aggregates, the incubation medium was centrifuged (3000 rpm for 30 min) and after separating the solid residue from the liquid, the former was dried in an oven at 60 °C for 24 h. The dry residue was dissolved in 125 μL of an ethylenediaminetetraacetic acid (EDTA) solution, which was prepared by dissolving 0.75 g of EDTA salt, previously dried at 80 °C for several hours, in 10 mL of PBS. Then, 100 μL of a blue dye called PR indicator, which forms a complex with Ca^{2+} ions, were added to confirm the presence of Ca^{2+} (*i.e.* PR is blue while Ca-PR is pink/red). The quantification of Ca^{2+} was performed adding a concentrated NaOH solution until the pH of the solution was 10. The UV spectrum was recorded, and the Ca^{2+} content was quantified using the calibration plot shown in Fig. S2, which was obtained using known concentrations of Ca^{2+} in the EDTA-containing PBS solution at pH 10.

The total Ca^{2+} concentration was estimated summing the concentration of Ca^{2+} detected in the incubation medium to the concentration of Ca^{2+} contained in Alg aggregates.

2.6. Electrochemical characterization

The electrical conductance retention was assessed by chronoamperometry (CA), that is, by measuring the time dependence of the current flowing through the hydrogels upon application of a constant voltage of 1.0 V as described below. An ITO-coated PET sheet of 2 × 3 cm^2 (Scheme 1a-1) was adapted by cutting a 2 mm wide strip of Kapton® tape and sticking it to the center of the longer side, dividing the ITO sheet in two parts (Scheme 1a-2). The rest of the surface was coated with nail polish (Scheme 1a-3). Once the nail polish was dry, the Kapton® strip was removed and the ITO sheet was subjected to treatment with aqueous hydrochloric acid (HCl) solution at 80 °C for 30 s, until the uncovered area loses conductivity (Scheme 1a-4). Subsequently, the nail polish was removed from the ITO sheet using sonication (Scheme 1a-5). A total of six cleaning steps (10 min each) were carried out using the following solvents for the sonication (in the order indicated): ethyl acetate, acetone, water with detergent, water, acetone and isopropanol.

Once the ITO sheet was prepared, the bottom of a syringe (1.3 cm diameter and 1.0 cm high) was cut, placed in the center of the ITO sheet, and joined to it using silicone (Scheme 1b). Subsequently, it was filled

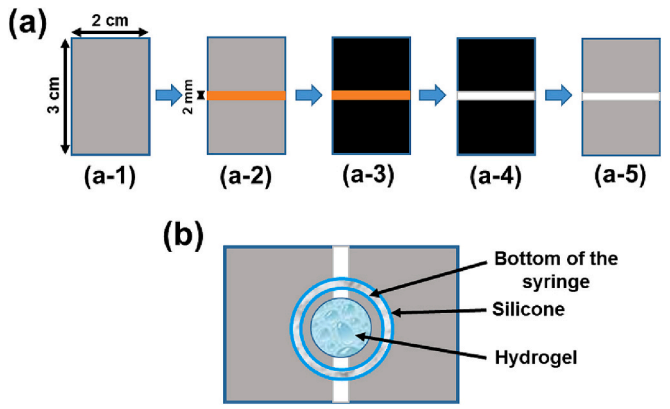

Scheme 1. (a) Process used to prepare an ITO sheet with two conductive halves separated by a non-conducting gap (2 mm wide). The different steps of the process are described in the text. (b) Set-up used for chronoamperometric measures.

with a hydrogel previously prepared in an identical mold (*i.e.* one formed by the bottom of a syringe joined to a flat surface) using the procedure previously described. Next, the hydrogel was coated with 1 mL of a PBS solution. Chronoamperometric measures were carried out applying to each sample ($n = 3$) a voltage of 1.0 V across the ITO gap for 1 h. After that time, the variation of the current density (j) against time was followed for 10 h.

Electrochemical activity was determined by cyclic voltammetry (CV) using a three-electrode cell and an Autolab PGSTAT302N. The examined hydrogels were used as working electrodes, while platinum and Ag|AgCl were used as counter and reference electrodes, respectively. Experiments were conducted in PBS (pH 7.4) at room temperature. The initial and final potentials were − 0.8 V, the reverse potential was +0.8 V, and the scan rate was 100 mV/s. Before the CV measurements, the hydrogels were incubated in the PBS solution for 5 min. All experiments were replicated at least 3 times using independent samples. Also, in order to stabilize the structure of the samples, five consecutive oxidation-reduction cycles were applied.

2.7. Electrochemical detection of hydrogen peroxide

Electrochemical detection of hydrogen peroxide (H_2O_2) was performed by CV using the set-up and operational parameters described in the previous sub-section. Once the structure of the hydrogel was stabilized with five redox cycles, cyclic voltammograms were recorded after adding different volumes of a H_2O_2 solution (30 wt%) to reach a final concentration in the range between 1 and 10 mM.

The limit of detection (LOD) and the limit of quantification (LOQ) for H_2O_2 were calculated as the ratio between k times the standard deviation of the blank (*i.e.* without H_2O_2) and the slope of the calibration curve with $k = 3$ and $k = 10$ for LOD and LOQ, respectively. All detection assays were replicated three times using independent samples.

2.8. Statistical analysis

Data points in graphics correspond to the average of samples and the error bars refer to the respective standard deviation. In addition, the Supplementary Information displays significant differences ($p < 0.05$) when 1 way ANOVA and Turkey's multiple comparison tests have been applied.

3. Results and discussion

3.1. Characterization

In addition to the broad band at 3360 cm^{-1} attributed to the O—H stretching, the FTIR spectra (Fig. 1a) of untreated and glyoxalized hydrogels show peaks at 1622 and 1432 cm^{-1} assigned to the asymmetric and symmetric C═O stretching, respectively, and bands at 1078 and 1010 cm^{-1} associated with the C–C–C and C–O–C stretching, respectively. In comparison to the C═O asymmetric stretching (reference), the relative intensity and relative broadness of the C–O–C band are higher for glyoxalized samples than for the untreated hydrogel, which we attribute to the expected formation of hemiacetal and acetal bonds during the glyoxalization process (Fig. 1b). Furthermore, comparison of the spectra recorded for PEDOT/Alg/G5, PEDOT/Alg/G30 and PEDOT/Alg/G120 indicates that, as expected, both the broadness and intensity of the peak associated with C–O–C relative to the C═O

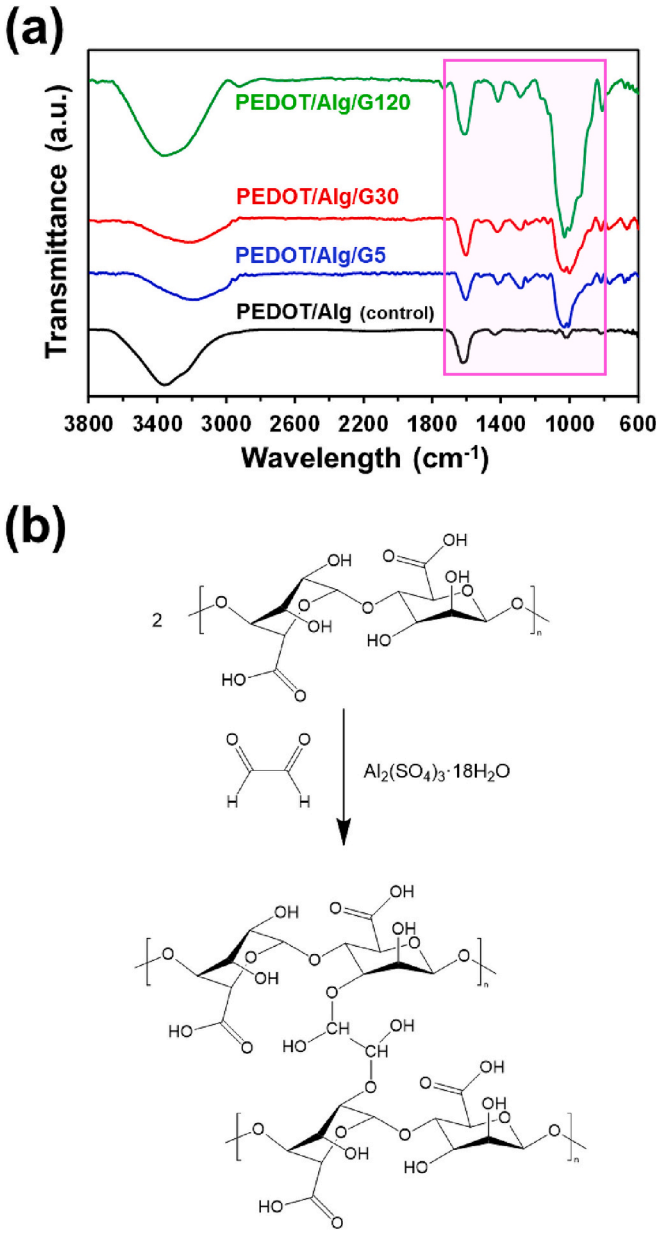

Fig. 1. (a) FTIR spectra of untreated PEDOT/Alg (control), PEDOT/Alg/G5, PEDOT/Alg/G30 and PEDOT/Alg/G120. (b) Crosslinking reaction between Alg and glyoxal.

asymmetric stretching increase with t_G (Fig. 1a).

In order to confirm the reaction mechanism proposed in Fig. 1b, covalently crosslinked Alg hydrogels (without semi-interpenetrated PEDOT:PSS) were prepared and studied by ^{1}H NMR spectroscopy. Fig. 2 compares the ^{1}H NMR spectra of untreated and glyoxalized Alg, the latter being prepared using $t_G = 30$ min (hereafter named Alg/G30). The ^{1}H NMR spectrum of Alg (Fig. 2a) shows the characteristic peaks (Huamani-Palomino, Córdova, Pichilingue, Venâncio, & Valderrama, 2021), as for example the anomeric proton of the α-L-guluronic (G) and β-D-mannuronic acid (M) residues at 5.03 and 4.64 ppm, respectively (signal **a** and **b**, respectively). Also, the peaks at 4.03, 3.74, 3.92 and 3.76 (signals **c**, **d**, **e** and **f**, respectively), which were assigned to the H2, H3, H4 and H5 of M residues, respectively, and those at 3.98, 4.19, 4.11 and 4.47 ppm (signals **g**, **h**, **i** and **j**, respectively), which were attributed to the H2, H3, H4 and H5 of G residues, respectively, are characteristic of Alg (Huamani-Palomino et al., 2021). The ^{1}H NMR spectrum recorded for Alg/G30 (Fig. 2b) reflected the success of the glyoxalization process, in which glyoxal formed a covalent crosslinked network between Alg chains. More specifically, four different resonance peaks appeared after the reaction in the region comprised between 4.88 and 5.52 pm (signals **k**–**n**), which were ascribed to signals from hemiacetal and acetal groups (Fig. 1b).

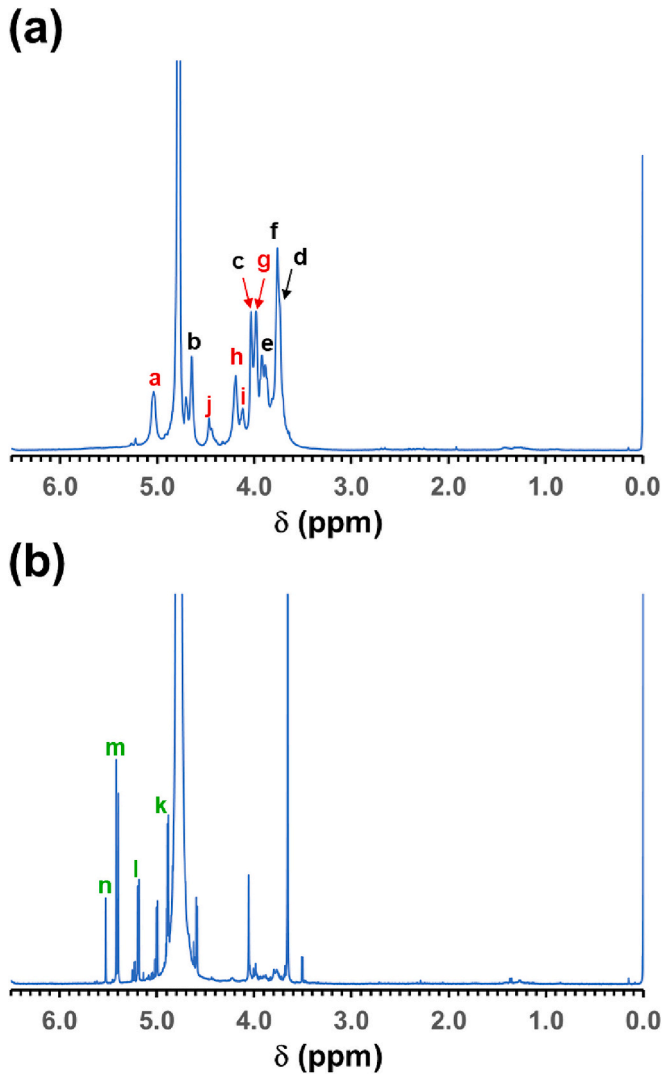

Fig. 2. ^{1}H NMR spectra of (a) Alg and (b) Alg/G30. Peaks labeled in red, black and green correspond to G residues, M residues and crosslinks, respectively. In (a) signals **a** and **b** were assigned to the anomeric proton of G and M, signals **c**, **d**, **e** and **f** to H2, H3, H4 and H5 of M residues, respectively, and signals **g**, **h**, **i** and **j** to the H2, H3, H4 and H5 of G residues. In (b) signals **k**–**n** were attributed to hemiacetal and acetal groups.

Furthermore, the successful reticulation of Alg with glyoxal was verified by ^{13}C NMR as well. ^{13}C NMR spectra of Alg and Alg/G30 are seen in Fig. 3. The absorption peak close to 180 ppm ($\delta = 177.5$ ppm) in the ^{13}C NMR spectrum of Alg was assigned to the carbon atom of carboxylate group, as previously reported (Işıklan, Kurşun, & İnal, 2010). Anomeric carbon resonance was observed at $\delta = 100.7$ ppm, while the peaks comprised between 65 and 85 ppm were for carbon atoms connected by –OH groups of the pyranose ring. In Alg/G30, the intensity of the band associated with pyronose carbon atoms bonded to –OH decreased while that associated to anomeric carbon atoms increased.

SEM micrographs of the cross-sections of PEDOT/Alg, PEDOT/Alg/G5 and PEDOT/Alg/G30 lyophilized hydrogels are displayed in Fig. 4a (micrographs of PEDOT/Alg/G60 and PEDOT/Alg/G120 are shown in Fig. S3). The cross-section of the untreated hydrogel shows an open and interconnected porous structure with a very wide distribution of pore sizes. However, the structure becomes less porous and shows a more compact matrix after treatment with glyoxal. Thus, small and medium size pores tend to disappear with increasing t_G. These phenomena, which can already be seen in PEDOT/Alg/G5 but are more evident for samples prepared using higher t_G (≥15 min), have been associated to the constraints imposed by the topology of the covalent crosslinks (*i.e.* constraints associated to covalent crosslinks are much more restrictive than those imposed Ca^{2+}-mediated crosslinks). Analysis of SEM micrographs using the ImageJ software ($n = 3$) indicated that the porosity of the untreated hydrogel decreased by 20 %–35 % after glyoxalization (depending on t_G).

The swelling of dry untreated and glyoxalized hydrogels is ascribed not only to the hydration of the hydrophilic groups of Alg and PEDOT, but also to the penetration of water molecules to fill the pores existing in the different hydrogel matrices. The swelling properties of the samples were tested in aqueous solutions. The temporal evolution of the SR (Eq. (1)) for 3 days in a 3 wt% $CaCl_2$ solution (Fig. 4b-left and Table S1) shows that it stabilizes in only 1 day, with a small increase up to day 3. This evolution may also reflect the diffusion of hydrated Ca^{2+} into the bulk of the hydrogel. As it can be seen, the SR increases by around 30 % (Table S1) when PEDOT/Alg is subjected to the shortest glyoxal treatment (PEDOT/Alg/G5), which is in fact the hydrogel showing the highest SR among the studied ones. This feature suggests that the glyoxalization process in PEDOT/Alg/G5 is incomplete, generating a significant amount of hydrophylic intermedium species that favors the incorporation of water (see below). The rest of the samples showed a SR that is not only lower than that of the control, but also decreases with t_G

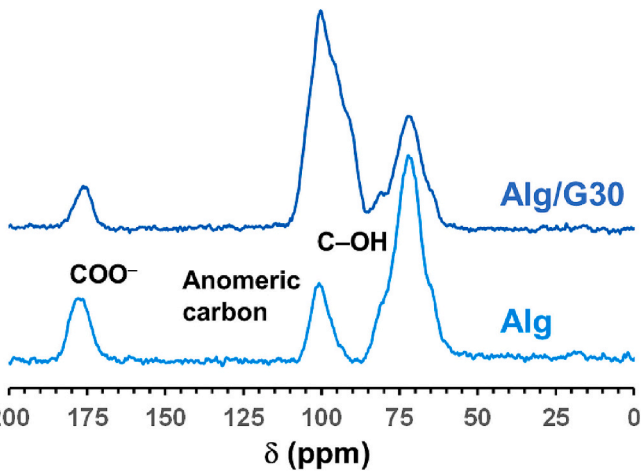

Fig. 3. Solid state ^{13}C NMR spectra of Alg and Alg/G30. The spectra were normalized with respect to the carboxylate signal ($\delta = 177.5$ ppm).

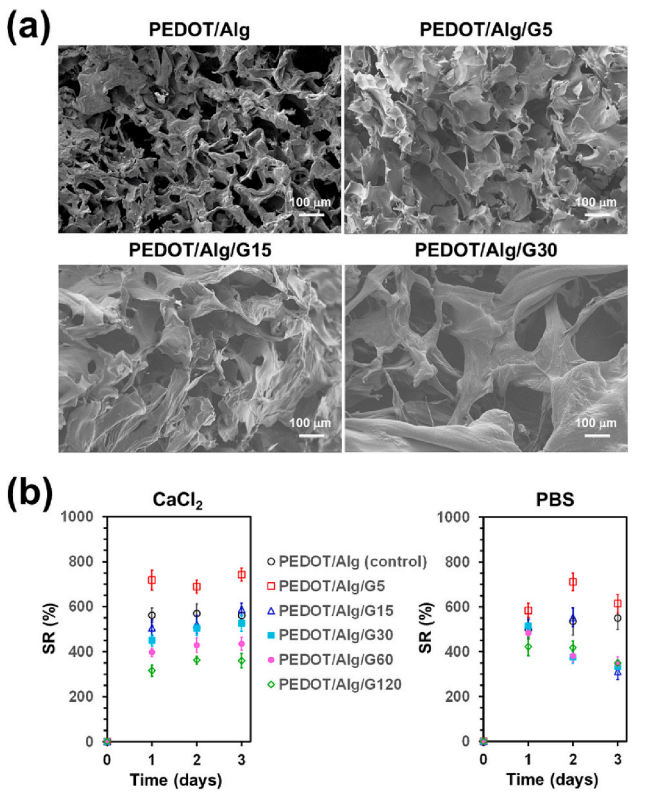

Fig. 4. (a) SEM micrographs of untreated PEDOT/Alg (control) and glyoxalized hydrogels prepared using a $t_G = 5$, 15 and 30 min. (b) Temporal evolution of the swelling ratio (SR) for the studied hydrogels in 3 wt% $CaCl_2$ solution (left) and in 0.01 M PBS solution.

(Table S1), a behavior that is consistent with SEM results, as the incorporation of covalent crosslinks results in more closed / compact structures.

A completely different behavior was observed in 0.01 M PBS, where the SR shows a more pronounced variation with time (Fig. 4b), especially for hydrogels prepared using $t_G = 15$, 30, 60 and 120 min. After 1 day, the water uptake of dried PEDOT/Alg/G15, PEDOT/Alg/G30, PEDOT/Alg/G60 and PEDOT/Alg/G120 led to SR values comprised between 423 % and 514 % (Table S1). However, after 3 days, the SR decreased to ~343 %. This change was attributed to the dynamics of the substitution of Ca^{2+} ions by monovalent cations coming from the dilute PBS solution. The closed structure of hydrogels prepared using $t_G \geq 15$ min made this substitution difficult, becoming a relatively slow process that results in the continuous formation and destruction of Ca^{2+}-mediated crosslinks, as those ions left the matrix. Instead, after 3 days, the swelling behavior of PEDOT/Alg/G5 was similar to that observed in the $CaCl_2$ solution, showing an SR that was 20 % higher than that of the untreated hydrogel (Table S1). The fact that the SR was systematically higher for PEDOT/Alg/G5 than for PEDOT/Alg supports that the former presents hydrophilic intermedium species. Overall, with the exception of the hydrogel obtained using the shortest t_G, the rest of hydrogels showed very similar SR values after 3 days that, as it was expected, were lower than that of untreated PEDOT/Alg. This feature indicates that the covalent network presents a more restricted topology than the ionic network, which causes a reduction in the porosity (as observed by SEM in Figs. 4a and S3) and, therefore, in the SR (Table S1, Fig. 4b).

Overall, Fig. 4b shows that the water absorption capacity of glyoxalized PEDOT/Alg hydrogels prepared using $t_G > 5$ min is lower than that of unmodified control samples. Thus, the presence of covalent crosslinks reduces the swelling capacity, as it was also reported for other polysaccharides crosslinked with glyoxal (Gupta & Jabrail, 2006; Quero et al., 2011). Moreover, covalent crosslinks affect the dynamical response of Ca^{2+}-mediated physical crosslinks, as it is shown by the temporal behavior of the SR in $CaCl_2$ solution, where ionic and covalent crosslinks coexist, and in PBS, where Ca^{2+} ions are replaced by monovalent cations.

To better understand the origin of the differences in the swelling of PEDOT/Alg/G5 with respect to other glyoxalized hydrogels, the surface free energy (SFE) of lyophilized samples was determined following the OWRK model. Although the values obtained, which are shown in Fig. 5a, do not have statistical significance, they show a trend that supports that PEDOT/Alg/G5 is more hydrophilic than the other glyoxalized hydrogels.

Fig. 5b displays the Young modulus (E) of non-treated and glyoxalized hydrogels as determined by quantitative nanomechanical AFM mapping. The Young modulus increases with t_G from 0.145 MPa for non-treated PEDOT/Alg to 0.230 MPa for PEDOT/Alg/G120, which evidences that the covalent network provides stiffness to the hydrogel. Considering that the reported E values for native soft tissues and organs range from 0.1 kPa to 1 MPa (Engler, Sen, Sweeney, & Discher, 2006; Hoenig et al., 2013), we can conclude that both non-treated and glyoxalized hydrogels exhibit biomimetic mechanical properties. For example, the different E values displayed in Fig. 5b match the mechanical features shown by muscle tissue (0.1–0.2 MPa) (Volpi, Paradiso, Costantini, & Święszkowski, 2022).

E is directly proportional to the density of crosslinks, and therefore increases with effective molecular weight. According to the rubber elasticity theory, which considered that each crosslink is a site from which four chain segments extend in different directions, the crosslink density (C_C, in moles per unit of volume) can be determined using E:

$$C_C = \frac{E}{6 \cdot R \cdot T} \tag{2}$$

where R is the molar gas constant (8.31 J/mol·K) and T is the absolute

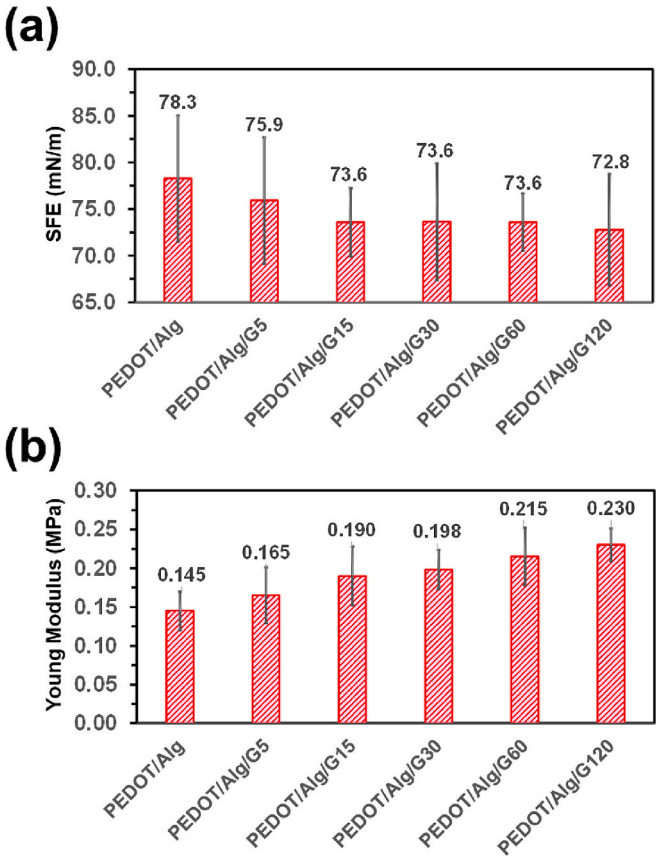

Fig. 5. (a) Surface free energy and (b) Young modulus of the studied hydrogels.

temperature (298 K). Table 1 shows that C_C grows with the glyoxalization time from $9.76{\cdot}10^{-9}$ mol/cm^3 (PEDOT/Alg) to $1.55{\cdot}10^{-8}$ mol/cm^3 (PEDOT/Alg/G120). The values of C_C have been converted into molecular weight between crosslinks (M_C; in g/mol) through the densities of untreated and glyoxalized hydrogels. Then, the mesh size, ξ, has been estimated using Eq. (3) from Canal and Peppas (1989):

$$\xi = \nu_S^{-1/3} \cdot L \sqrt{\frac{2 \cdot C_n \cdot M_C}{M_r}} \tag{3}$$

where ν_S is the polymer volume fraction in the equilibrium swollen state, L is the bond length along the polymer backbone (~ 0.15 nm); C_n is the Flory characteristic ratio (taken as 21.1 for Alg, according to Lee, Li, & Guelcher, 2021); and M_r is the molecular weight of the repeat unit (194.14 g/mol). Following the approach of Schwartz et al. (2010) the contributions of the glyoxal crosslinkers to C_n and M_r were neglected, which is a reasonable assumption as the hydrogel networks are predominantly Alg. The value of ν_S, has been estimated as the inverse of the weight swelling fraction (*SF*), which corresponds to the mass of swollen hydrogel at equilibrium (w_S) divided by the weight of the dry hydrogel (w_D):

$$\upsilon_S = \frac{1}{SF} = \frac{w_D}{w_S} \tag{4}$$

The value of SF is smaller for all glyoxalized hydrogels than for untreated PEDOT/Alg with exception of PEDOT/Alg/G5 (Table 1) that, as was mentioned above, is the most hydrophylic because of the intermediate species. Finally, the estimated mesh size, which decreased ~44 % for PEDOT/Alg/G5 with respect to untreated PEDOT/Alg, showed a slight reduction of up to 49 % when the t_G increased to 120 min.

3.2. Dual crosslinking network

Glyoxalized PEDOT/Alg hydrogels are expected to exhibit a dual crosslinking network in which glyoxal-mediated covalent crosslinks coexist with Ca^{2+}-mediated ionic crosslinks between Alg G-blocks. However, the amount of ionic crosslinks is expected to depend on t_G, decreasing with increasing t_G. In order to confirm such dependence, the content of Ca^{2+} in the hydrogels was determined using UV–Vis spectroscopy. More specifically, hydrogel samples were incubated in PBS for a period of 1 h (0 day), 1 day and 7 days, promoting the substitution of Ca^{2+} by monovalent ions (Na^+ and K^+). After each of such periods, the incubation medium was replaced by a fresh one while the removed PBS, to which PR indicator was added, was used for analysis with UV–Vis spectroscopy. Fig. 6a–b compares the UV–Vis spectra recorded for untreated PEDOT/Alg (control) and PEDOT/Alg/G30 after each incubation period, while the spectra obtained for PEDOT/Alg/G5, PEDOT/Alg/G15, PEDOT/Alg/G60 and PEDOT/Alg/G120 are displayed in Fig. S4.

Quantification of the released Ca^{2+} ions into the PBS medium was performed using calibration plots, as described in the Methods section. Two calibration plots were obtained from the peaks at λ = 464 nm and 636 nm present in the UV–Vis spectra recorded for PBS solutions with known Ca^{2+} concentrations (Fig. S1a). The peak at λ = 566 nm was discarded because it shifted towards lower wavelengths with increasing Ca^{2+} concentration. However, as the correlation coefficient was higher for the plot derived from the peak at λ = 464 nm (Fig. S1b) than for the one at λ = 636 nm (Fig. S1c), the former was chosen for quantification. The absorbance of non-crosslinked Alg (*i.e.* without Ca^{2+}), glyoxal and PEDOT:PSS at λ = 464 nm is negligible (Fig. S5). Fig. 6c shows the Ca^{2+} concentration released from the hydrogels to the incubation medium. As it can be observed, Ca^{2+} concentration increased with time, independently of t_G, which evidences the presence of a dual crosslinking network for all glyoxalized hydrogels. However, the most noticeable result was that, as it was expected, the concentration of released Ca^{2+} ions decreased with t_G, especially for $t_G > 15$ min. Thus, the amount of Ca^{2+} released from PEDOT/Alg/G30, PEDOT/Alg/G60 and PEDOT/Alg/G120 hydrogels to the PBS medium after 7 days was smaller than the one from PEDOT/Alg by 55 %, 60 % and 63 %, respectively.

The turbidity of the incubation medium, which increased with the incubation time, and the structural damage of the untreated and some glyoxalized hydrogels, which was visually observed, were attributed to the partial loss of the ionic crosslinking network. Thus, the replacement of Ca^{2+} ions by monovalent ions coming from the PBS solution was accompanied by the release of aggregates formed by Alg chains that were insufficiently crosslinked in the covalent network of the hydrogel. The released aggregates were separated as solid residues by centrifugation and, after drying, were re-suspended in an EDTA-containing PBS solution to quantify the content of Ca^{2+}, whose presence was previously confirmed using the PR indicator (see Methods section). The UV–Vis spectra of the solutions coming from the residues of PEDOT/Alg and PEDOT/Alg/G30 hydrogels are shown in Fig. 7a–b, while those coming from the residues of the hydrogels prepared using t_G = 5, 15, 60 and 120 min are displayed in Fig. S6. The quantification of Ca^{2+} in the EDTA-containing solution (Fig. 7c) was performed using the calibration plot obtained with known Ca^{2+} concentrations (Fig. S2b) and measuring the intensity of the peak recorded at λ = 589 nm.

Fig. 7d displays the total Ca^{2+} concentration, which was obtained by summing the concentration of Ca^{2+} directly released to the PBS medium (Fig. 6c) and the concentration of Ca^{2+} extracted from Alg aggregates using an EDTA-containing PBS solution (Fig. 7c). For all studied systems, the concentration of Ca^{2+} increased with the incubation time, even though the total value was approximately twice for the non-treated hydrogel than for the glyoxalized ones. On the other hand, the influence of the t_G value on the total content of Ca^{2+} was apparently less critical than expected. Thus, all hydrogels obtained using $t_G \geq 30$ min showed a very similar content of Ca^{2+}, while PEDOT/Alg/G15 showed a little more Ca^{2+} content but without being a very notable difference with respect to PEDOT/Alg/G30. Overall, these results indicate that the dual crosslinking network is preserved for all glyoxalized hydrogels, even for those prepared using t_G = 60 and 120 min.

The concentration of Ca^{2+} recovered from Alg aggregates (Fig. 7c), which was lower than that directly released to the incubation medium (Fig. 6c), was higher for PEDOT/Alg than for glyoxalized hydrogels and increased with time. For example, the amount of Ca^{2+} extracted from Alg aggregates after 1 day was 26 % higher for PEDOT/Alg than for PEDOT/Alg/G5, and such difference increased to 95 % after 7 days. This has been attributed to the combination of a lower Ca^{2+} content in the glyoxalized hydrogels (we expect that some Ca^{2+} would have diffused out during the treatment with glyoxal) and a lower diffusivity of these ions upon increase of the hydrogel compactness upon covalent crosslinking.

On the other hand, the gel fraction (*GF*) was determined to evaluate the efficiency of the chemical crosslinking. The *GF* has been expressed as follows:

$$GF = \frac{m_d}{m_e} \cdot 100 \tag{5}$$

where m_d is the mass of the dried hydrogel after chemical crosslinking and m_e is the mass of the dried hydrogel after extraction of uncrosslinked material. It is worth noting that *GF* contains the contribution of both

Table 1
Mesh properties determined for untreated and glyoxalized hydrogels: Average crosslink density (C_C), average swelling fraction (*SF*) and mesh size (ξ).

	C_C (mol/cm^3)	*SF*	ξ (nm)
PEDOT/Alg	$9.76{\cdot}10^{-9}$	6.50	7.1 ± 0.3
PEDOT/Alg/G5	$1.11{\cdot}10^{-8}$	7.14	4.0 ± 0.1
PEDOT/Alg/G15	$1.28{\cdot}10^{-8}$	4.12	4.2 ± 0.2
PEDOT/Alg/G30	$1.33{\cdot}10^{-8}$	4.33	4.1 ± 0.1
PEDOT/Alg/G60	$1.45{\cdot}10^{-8}$	4.45	3.7 ± 0.1
PEDOT/Alg/G120	$1.55{\cdot}10^{-8}$	4.50	3.6 ± 0.1

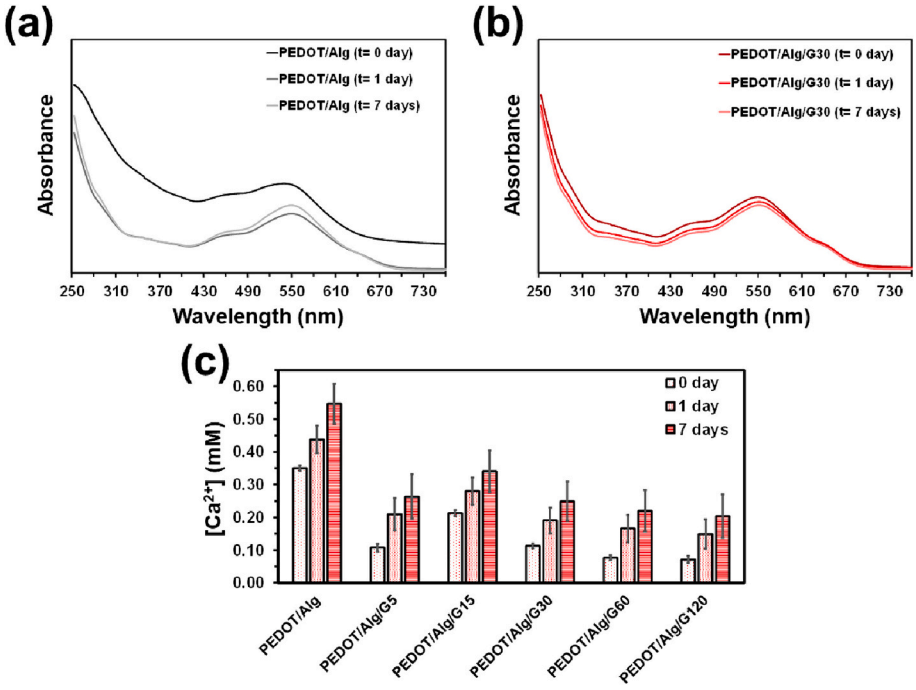

Fig. 6. UV–Vis spectra of the PBS medium after incubating the (a) PEDOT/Alg and (b) PEDOT/Alg/G30 hydrogels for 1 h (0 day), 1 day and 7 days. Spectra for the rest of hydrogels are shown in Fig. S4. (c) Quantification of the Ca^{2+} released to the medium using the calibration plot displayed in Fig. S1b (λ = 464 nm).

Ca^{2+}- and glyoxal-mediated crosslinks. The *GF* obtained for the hydrogels prepared using t_G = 5, 15, 30, 60 and 120 min was 92 %, 89 %, 86 %, 85 % and 83 %, which is consistent with the variation in the Ca^{2+} content previously discussed.

3.3. Electrochemical characterization

The electrochemical response of untreated and glyoxalized hydrogels was firstly studied by CA using the set-up described in the Methods section (Scheme 1). A voltage of 1.0 V was applied to each hydrogel across the ITO gap for 1 h and, subsequently, the evolution of the current density (*j*) with time was examined to determine the current, and therefore the conductance, retention at that voltage. Results for as prepared PEDOT/Alg samples, which are shown in Fig. 8a, indicate that *j* stabilizes at values below 0.015 μA/cm^2 after ~5 h, while glyoxalized hydrogels exhibit higher current retention capacity. Indeed, glyoxalized samples can be categorized in two groups: 1) those prepared using $t_G \geq$ 60 min, which retain *j* values higher than 0.15 μA/cm^2 after 10 h; and 2) those prepared using $t_G <$ 60 min, which retain *j* values comprised between 0.030 and 0.065 μA/cm^2, depending on t_G. Interestingly, for the last group, no correlation was found between current retention and the t_G. Moreover, repetitions showed variability and lack of reproducibility, even though in all cases the *j* values after 10 h were comprised between 0.028 and 0.065 μA/cm^2. This observation suggests that the glyoxalization process was not complete for PEDOT/Alg/G5, PEDOT/Alg/G15 and PEDOT/Alg/G30 samples. Instead, the glyoxalization process was complete or almost complete for PEDOT/Alg/G60 and PEDOT/Alg/G120, which exhibited reproducibility, higher current retention and, therefore, higher conductance retention. In view of the dc type of voltage and its low value (1.0 V), which does not promote the water electrolysis, the ITO electrodes behave as blocking electrodes, and the stabilized current and conductance must be of electronic origin only.

In order to examine the current retention stability, hydrogels were immersed for 24 h and 7 days in PBS. After those time intervals, hydrogels were again electrically stimulated applying a voltage of 1.0 V for 1 h and the temporal evolution of *j* with time was monitored (Fig. 8b–c). Results showed that, as it was expected, the current retention of untreated PEDOT/Alg was practically null, *j* decreasing to values lower than 0.001 μA/cm^2 after 10 h. Thus, the stability of the untreated hydrogel was severely damaged in PBS due to the substitution of Ca^{2+} by monovalent cations. Immersion in PBS of glyoxalized hydrogels obtained using $t_G <$ 60 min also caused a drastic reduction in *j*, which decreased to 0.02–0.05 and 0.005–0.03 μA/cm^2 after 24 h and 7 days in PBS, respectively. Conversely, the current retention of PEDOT/Alg/G60 and PEDOT/Alg/G120 was higher than 0.07 μA/cm^2, even after 7 days of immersion in PBS. These results illustrate the importance of the covalent network in the electrical response of glyoxalized hydrogels. The nearly steady state current reached upon 1 h stimulation, ascribed to electronic transport, which is higher for the samples with longer glyoxal treatment (*i.e.* t_G of 60 and120 min), suggests that electronic charge percolation is more effective for these samples, which is likely due to changes in the hydrogels microstructure, promoting a higher connectivity of the conductive PEDOT domains.

CV is *a* potentiodynamic electrochemical technique that involves the cyclic *scan* of *potential* while measuring current. It is worth noting that hydrogels can undergo structural deformations, such as swelling, shrinkage, and bending, in response to the potential scanning process. This is due to the fact that during the application of forward and back scans, the entrance and escape of hydrated ions from the polymeric matrix require the rapid re-accommodation of the polymer chains in the hydrogel, which is sometimes difficult because of the crosslinking nature. The current response of untreated and glyoxalized hydrogels was studied by CV using a potential interval ranging from −0.80 V to +0.80 V at a scan rate of 100 mV/s.

Firstly, the structure of the hydrogel was stabilized applying four consecutive CV cycles in PBS. After that, the fifth cyclic voltammogram was recorded, as shown in Fig. 9. The voltammogram obtained for untreated PEDOT/Alg exhibited a significant area, which was fully consistent with the re-accommodation of the polymer chains in the hydrogel matrix after several potential scans. Such re-arrangement was facilitated by the ionic nature of the crosslinks through the redistribution of the Ca^{2+} ions. The area of the fifth voltammogram increased considerably for PEDOT/Alg/G5, indicating that the formation of a low amount of covalent crosslinks not only facilitated the re-accommodation

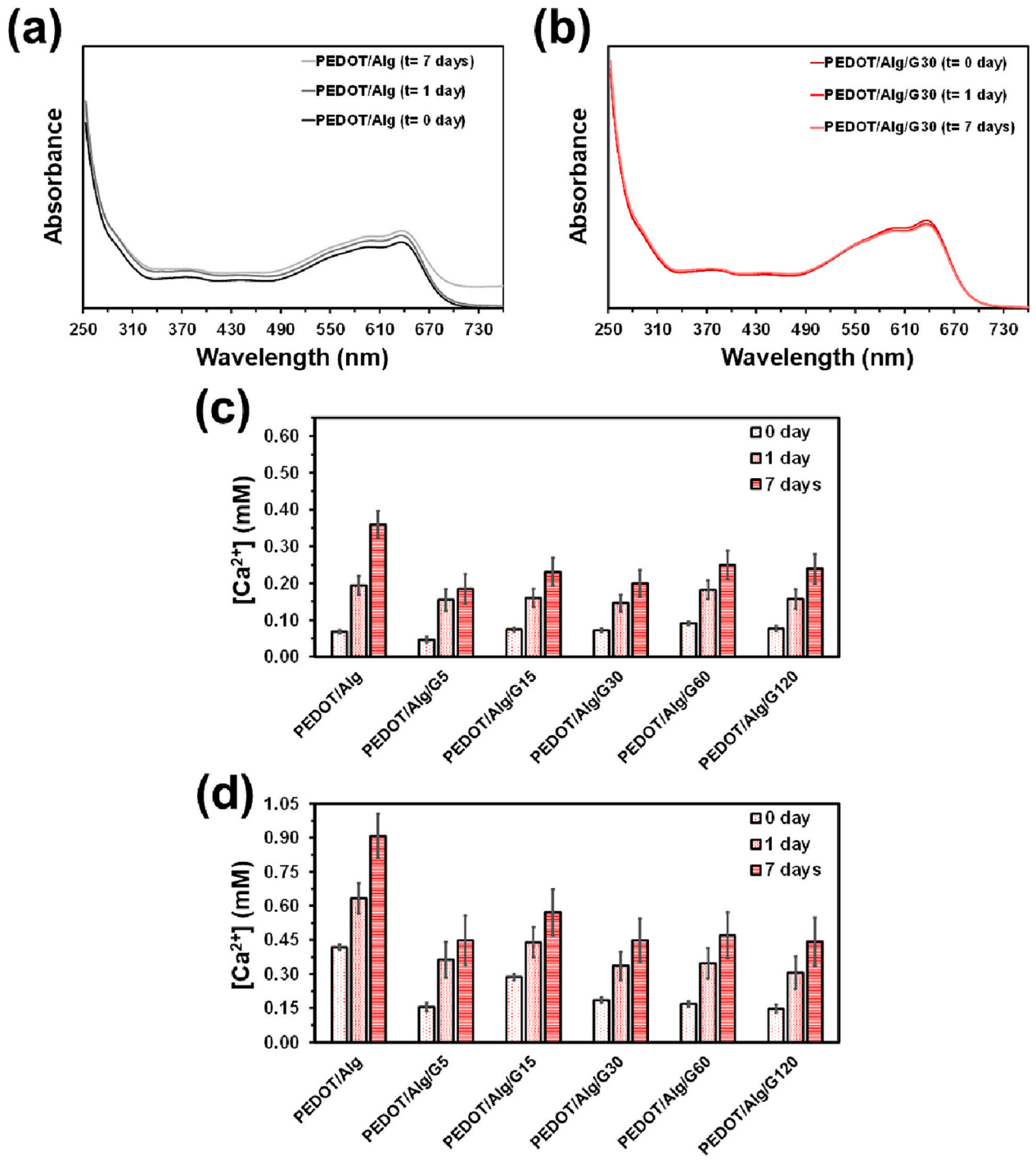

Fig. 7. UV–Vis spectra of the EDTA-containing PBS solution prepared using Alg aggregates (*i.e.* solid residues) released from (a) PEDOT/Alg and (b) PEDOT/Alg/G30 hydrogels and incubated for 1 h (0 day), 1 day and 7 days. Spectra for the rest of hydrogels are shown in Fig. S6. (c) Quantification of the Ca^{2+} released to the medium using the calibration plot displayed in Fig. S2b ($\lambda = 589$ nm). (d) Total content of Ca^{2+} in non-treated and glyoxalized hydrogels, which was estimated by adding the values displayed in Figs. 6c and 7c.

of the polymer chains and the re-organization of Ca^{2+} ions, but also avoided any loss of material during the entrance and scape of counter-ions. Conversely, the area of the voltammograms decreased progressively with increasing amount of covalent crosslinks for $t_G > 5$ min, the smallest area being obtained for PEDOT/Alg/G120. This was attributed to the conformational constraints imposed by the growing amount of covalent crosslinks, which was enhanced by the small size of the glyoxal crosslinker. Thus, the re-accommodation of the Alg and PEDOT chains became hindered by the covalent crosslinks, which affected the electrochemical activity of the semi-interpenetrated hydrogel.

Overall, the results indicate that the robustness of the electrochemical measures determined in PBS is much higher for the hydrogels with dual crosslinking than for untreated PEDOT/Alg. Thus, the structure of glyoxalized hydrogels is stable, even after being immersed in PBS for several days. Furthermore, the current retention and the electrochemical activity increases and decreases, respectively, with increasing degree of glyoxalization, which have been attributed to the topological restrictions imposed by glyoxal that affect the porosity and, therefore,

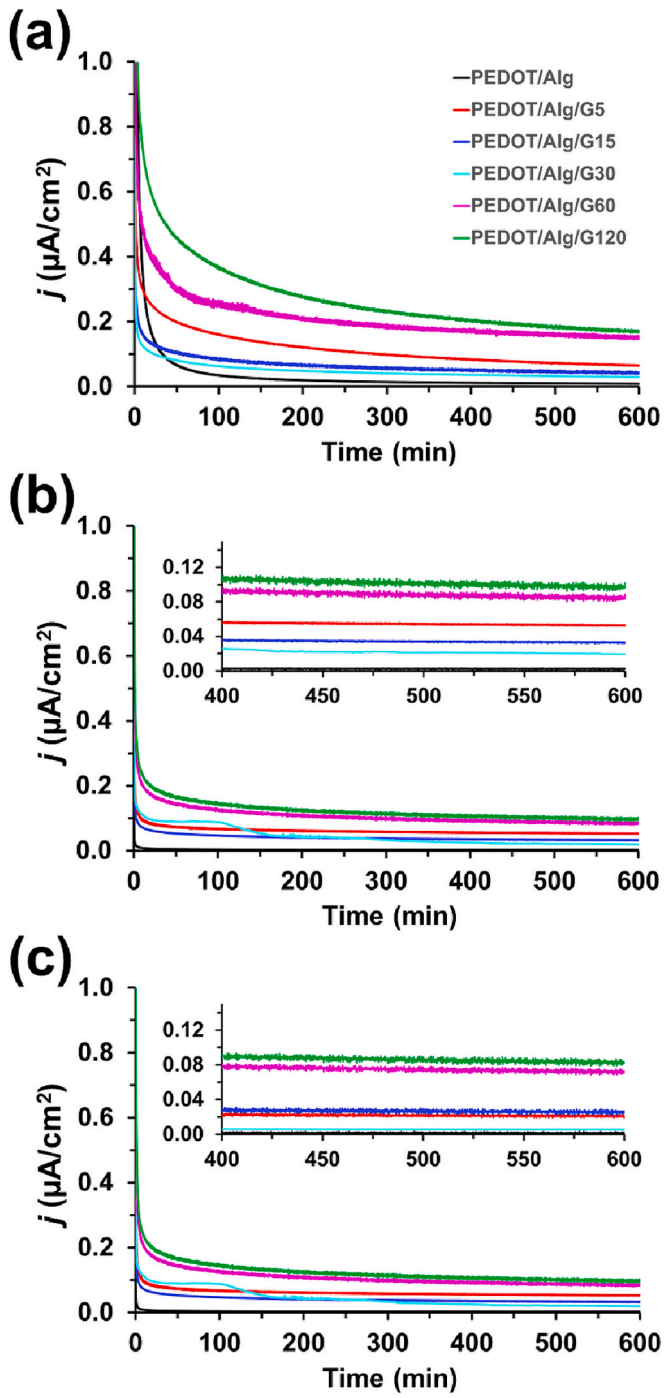

Fig. 8. Chronoamperometric results obtained for untreated and glyoxalized hydrogels: (a) as prepared; (b) after 24 h immersed in PBS; and (c) after 7 days immersed in PBS. Time "t = 0 min" corresponds to the instant at which the voltage has been applied for 60 min.

the charge transport.

3.4. Detection of hydrogen peroxide

In previous sub-sections, we have demonstrated that the morphological, mechanical, swelling, electrical and electrochemical properties of glyoxalized PEDOT/Alg hydrogels can be regulated by fixing the value of t_G. Here, we show how this control can be used for tuning the behavior of such hydrogels, improving their performance when used in a given application. Although different applications have been proposed

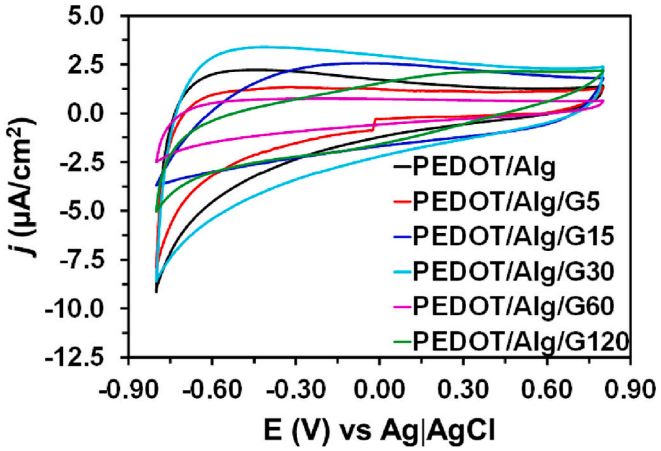

Fig. 9. Voltammograms (fifth redox cycle) obtained for untreated and glyoxalized hydrogels in PBS. The initial and final potentials were −0.8 V, the reversal potential was +0.8 V, and the scan rate was 100 mV/s.

for PEDOT/Alg hydrogels (Puiggalí-Jou et al., 2021), in this sub-section we have focused on their utilization as flexible electrodes for the electrochemical detection of H_2O_2, an analyte that comes from many metabolic processes, using CV. The basis for this choice is that the potentiodynamic response of glyoxalized hydrogels is precisely the least versatile (Fig. 9).

The response of untreated and glyoxalized hydrogels to the addition of H_2O_2 to the PBS medium was studied by CV. For this purpose, hydrogels were pre-stabilized in PBS by applying four consecutive redox cycles and, subsequently, the H_2O_2 concentration was progressively increased to 1, 2, 5, 7.5 and, finally, 10 mM. A cyclic voltammogram was recorded after each H_2O_2 addition. The voltammograms recorded for untreated PEDOT/Alg and PEDOT/Alg/G5 hydrogels (Fig. 10a–b) show that the addition of H_2O_2 led to significant changes in the current density at −0.80 V, which was attributed to the electrochemical reduction of H_2O_2(aq) to OH^-(aq). More specifically, the current density clearly increased (in absolute value) with increasing concentration of H_2O_2, changing from −9 μA/cm^2 (0 mM H_2O_2) to −20 μA/cm^2 (10 mM H_2O_2) for PEDOT/Alg and from −8 μA/cm^2 (0 mM H_2O_2) to −32 μA/cm^2 (10 mM H_2O_2) for PEDOT/Alg/G5. According to such results, the potential used to monitor the reduction of H_2O_2 to OH^- was −0.80 V, in good agreement with the literature (Babeli et al., 2021).

Fig. 11a–b represents the current density at −0.80 V *versus* the concentration of H_2O_2 for PEDOT/Alg and PEDOT/Alg/G5. Both calibration plots, which were obtained using three independent repetitions for each H_2O_2 concentration, show that the current density (in absolute value) at −0.8 V linearly increases with increasing H_2O_2 concentration (R^2 = 0.9936 and 0.9582, respectively). The sensitivity towards H_2O_2, which was defined by the slope (in absolute value) of such plot, is higher for PEDOT/Alg/G5 than for untreated PEDOT/Alg (Table 2), which has been attributed to the higher electrochemical activity of the former hydrogel. Furthermore, the LOD (signal-to-noise ratio 3:1) and LOQ (signal-to-noise ratio 10:1) were one order of magnitude lower for PEDOT/Alg/G5 than for PEDOT/Alg (Table 2). This feature was attributed not only to the differences in the electroactivity, but also to the low standard deviations obtained for the blank (*i.e.* reproducibility of the voltammograms recorded without H_2O_2). Also, Fig. 11a–b reveals very low standard deviations, reflecting that the detection of H_2O_2 reduction was very reproducible.

The performance of flexible sensors for H_2O_2 detection was recently reviewed (Giaretta et al., 2022). The statistical parameters displayed in Table 2 for PEDOT/Alg/G5 are better than those reported for many enzymatic and non-enzymatic carbonaceous and polymeric electrodes. For example, enzymatic electrodes made of chitosan/gelatin composite functionalized with horse radish peroxidase and graphene

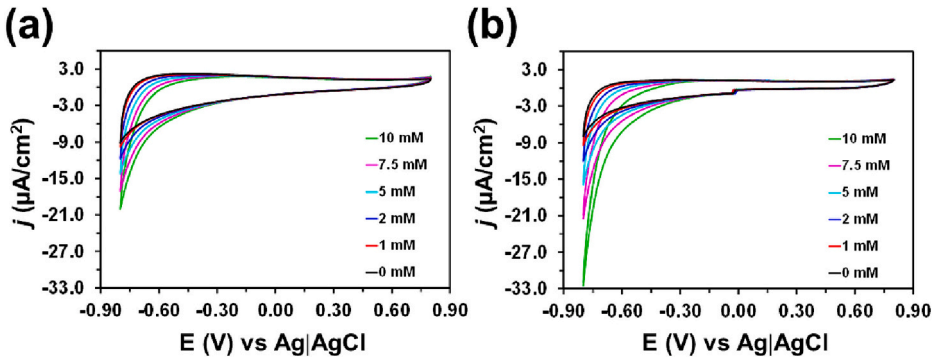

Fig. 10. Voltammograms recorded in PBS with increasing concentration of H_2O_2 (1–10 mM) after stabilizing the hydrogel with four redox cycles: (a) PEDOT/Alg; and (b) PEDOT/Alg/G5. Scan rate: 100 mV/s.

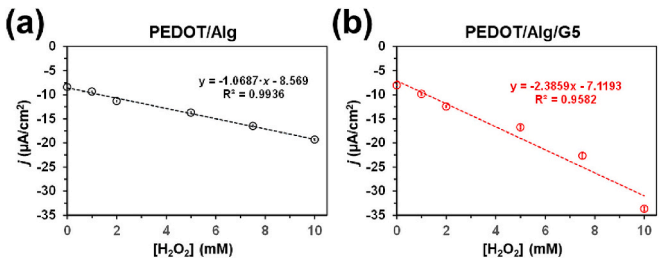

Fig. 11. Calibration plots representing the current density at −0.80 V *versus* the concentration of H_2O_2 for: (a) untreated PEDOT/Alg; and (b) PEDOT/Alg/G5.

Table 2
Sensitivity, limit of detection (LOD) and limit of quantification (LOQ) for the detection of H_2O_2 using PEDOT/Alg and PEDOT/Alg/G5. Values were extracted from the cyclic voltammograms and calibration plots displayed in Figs. 10a–b and 11a–b, respectively.

	Sensitivity (μA/mmol·cm^{-2})	LOD (mM)	LOQ (mM)
PEDOT/Alg	1.069	0.241	0.802
PEDOT/Alg/G5	2.386	0.018	0.060

functionalized with peroxidase from guinea grass exhibit a LOD of 0.05 mM (Teepoo, Dawan, & Barnthip, 2017) and 0.15 mM (Centeno, Solano, & Castillo, 2017), respectively, while platinum nanoflowers and activated glassy carbon showed a LOD of 0.06 mM (Wan, Wang, Yin, & Ma, 2012) and 0.053 mM (Murugan et al., 2022), respectively.

As it was expected, the electrochemical response of glyoxalized hydrogels prepared using $t_G \geq 5$ min was practically independent of the concentration of H_2O_2 (Fig. S7). Accordingly, the slope of the plots representing the current density at −0.80 V *versus* the concentration of H_2O_2 was close to zero, as is reflected in Fig. S8.

Overall, the results obtained in this sub-section indicate that the CV-mediated detection capacity of PEDOT/Alg glyoxalized hydrogels largely depends on t_G. More specifically, the sensing performance of untreated PEDOT/Alg is considerably enhanced when a low fraction of covalent crosslinks is incorporated by applying $t_G \leq 5$ min. Nevertheless, the conformational restraints imposed by the covalent crosslinks created using $t_G > 5$ min are detrimental for the sensing capacity, which has been attributed to the difficulties in the re-accommodation of the polymer chains during the redox cycles.

4. Conclusions

In this study, electro-responsive glyoxalized PEDOT/Alg hydrogels were developed. Glyoxal, the shortest dialdehyde ($C_2H_2O_2$), was used to create covalent crosslinks between the Alg chains leading, in combination with Ca^{2+}-mediated ionic crosslinks, to the formation of dual network hydrogels. The density of covalent crosslinks increased with t_G, while the amount of Ca^{2+}-mediated crosslinks decreased. The physical properties (*i.e.* morphology, Young modulus, swelling behavior, current retention capacity and electrochemical activity) can be regulated through t_G. In comparison with untreated PEDOT/Alg, the Young modulus and current retention capacity of glyoxalized hydrogels increased with t_G, while the porosity, swelling behavior and electrochemical activity decreased with increasing t_G. In general, the behavior of PEDOT/Alg/G5 was discordant with those tendencies, which was attributed to the fact that the glyoxalization process was in its early stages, and a significant amount of hydrophilic intermediate species were formed. Therefore, the dependence of the properties on the degree of glyoxalization can be used to modify the properties of PEDOT/Alg on demand and tune its performance towards different applications. The benefits of glyoxalization were demonstrated comparing the performance of untreated PEDOT/Alg and PEDOT/Alg/G5 as a flexible electrode for detecting H_2O_2. Results showed that the sensitivity doubled and LOD and LOQ were one order of magnitude smaller for the glyoxalized hydrogel. We believe that the glyoxalization of PEDOT/Alg offers an optimization platform for such versatile hydrogel.

CRediT authorship contribution statement

Samuele Colombi: Writing – review & editing, Visualization, Validation, Methodology, Investigation, Formal analysis, Data curation. **Isabel Sáez:** Writing – review & editing, Validation, Investigation, Data curation. **Nuria Borras:** Writing – review & editing, Investigation. **Francesc Estrany:** Writing – review & editing, Investigation. **Maria M. Pérez-Madrigal:** Writing – review & editing, Investigation. **José García-Torres:** Writing – review & editing, Validation, Supervision, Resources, Methodology, Investigation, Funding acquisition, Data curation, Conceptualization. **Jorge Morgado:** Writing – review & editing, Validation, Supervision, Resources, Project administration, Methodology, Investigation, Formal analysis, Conceptualization. **Carlos Alemán:** Writing – original draft, Visualization, Supervision, Resources, Project administration, Investigation, Funding acquisition, Formal analysis, Conceptualization.

Declaration of competing interest

The authors declare that they have no known competing financial interests or personal relationships that could have appeared to influence the work reported in this paper.

Data availability

Data will be made available on request.

Acknowledgements

This publication is part of the I+D+i project PID2021-125767OB-I00 and PLEC2022-009279 funded by MCIN/AEI/10.13039/501100011033 and by "ERDF A way of making Europe", by the European Union. Authors are thankful to the Agència de Gestió d'Ajuts Universitaris i de Recerca (2021 SGR 00387 and 2021 SGR 01368) for financial support. JM thanks FCT financial support under the project UIDB/50008/2020. M.M.P.-M. thanks the Ministerio de Ciencia, Innovación y Universidades for the Junior Beatriz Galindo Award (BG20/00216). J.G.-T. acknowledges the Serra Hunter program of the Generalitat de Catalunya. Support for the research of C.A. was also received through the prize "ICREA Academia" for excellence in research funded by the Generalitat de Catalunya. S.C. thanks the Agència de Gestió d'Ajuts Universitaris i de Recerca (AGAUR; Generalitat de Catalunya) for a FI Fellowship.

Appendix A. Supplementary data

Supplementary data to this article can be found online at https://doi.org/10.1016/j.carbpol.2024.122170.

References

Alabi, A., Aubry, C., & Zou, L. (2022). Graphene oxide-alginate hydrogel for drawing water through an osmotic membrane. *ACS Omega, 7*, 38337–38346.

Babeli, I., Puiggalí-Jou, A., Josep Roa, J., Ginebra, M. P., García-Torres, J., & Alemán, C. (2021). Hybrid conducting alginate-based hydrogel for hydrogen peroxide detection from enzymatic oxidation of lactate. *International Journal of Biological Macromolecules, 193*, 1237–1248.

Babeli, I., Ruano, G., Casanovas, J., Ginebra, M. P., García-Torres, J., & Alemán, C. (2020). Conductive, self-healable and reusable poly (3, 4-ethylenedioxythiophene)-based hydrogels for highly sensitive pressure arrays. *Journal of Materials Chemistry C, 8*, 8654–8667.

Bajpai, S. K., & Sharma, S. (2004). Investigation of swelling/degradation behavior of alginate beads crosslinked with Ca^{2+} and Ba^{2+} ions. *Reactive and Functional Polymers, 59*, 129–140.

Bogdanova, L. R., Zelenikhin, P. V., Makarova, A. O., Zueva, O. S., Salnikov, V. V., Zuev, Y. F., & Ilinskaya, O. N. (2022). Alginate-based hydrogel as delivery system for therapeutic bacterial RNase. *Polymers, 14*, 2461.

Braccini, I., & Pérez, S. (2001). Molecular basis of Ca^{2+}-induced gelation in alginates and pectins: The egg-box model revisited. *Biomacromolecules, 2*, 1089–1096.

Canal, T., & Peppas, N. A. (1989). Correlation between mesh size and equilibrium degree of swelling of polymeric networks. *Journal of Biomedical Materials Research, 23*, 1183–1193.

Cao, N., Chen, X. B., & Schreyer, D. J. (2012). Influence of calcium ions on cell survival and proliferation in the context of an alginate hydrogel. *ISRN Chem. Eng., 2012*, Article 516461.

Castro, C., Cordeiro, N., Faria, M., Zuluaga, R., Putaux, J.-L., Filpponen, I., … Gañán, P. (2015). In-situ glyoxalization during biosynthesis of bacterial cellulose. *Carbohydrate Polymers, 126*, 32–39.

Centeno, D. A., Solano, X. H., & Castillo, J. J. (2017). A new peroxidase from leaves of guinea grass (Panicum maximum): A potential biocatalyst to build amperometric biosensors. *Bioelectrochemistry, 116*, 33.

Chen, F., Monnier, X., Gällstedt, M., Gedde, U. W., & Hedenqvist, M. S. (2014). Wheat gluten/chitosan blends: A new biobased material. *European Polymer Journal, 60*, 186–197.

Da Silva, A. C., Wang, J., & Minev, I. R. (2022). Electro-assisted printing of soft hydrogels via controlled electrochemical reactions. *Nature Communications, 13*, 1353.

Dey, A., Bera, B., Bera, R., & Chakrabart, D. (2014). Influence of diethylene glycol as a porogen in a glyoxal crosslinked polyvinyl alcohol hydrogel. *RSC Advances, 4*, 42260–42270.

Du, X., Yang, L., & Liu, N. (2023). Recent progress on poly(3,4-ethylenedioxythiophene): Poly(styrenesulfonate) bioelectrodes. *Small Science, 3*, Article 2300008.

Eiselt, P., Lee, K. Y., & Mooney, D. J. (1999). Rigidity of two- component hydrogels prepared from alginate and poly(ethyleneglycol)−diamines. *Macromolecules, 32*, 5561–5566.

Elsayed, N. H., Monier, M., Alatawi, R. A. S., Albalawi, M. A., & Alhawiti, A. S. (2022). Preparation of chromium (III) ion-imprinted polymer based on azo dye functionalized chitosan. *Carbohydrate Polymers, 284*, Article 119139.

Engler, A. J., Sen, S., Sweeney, H. L., & Discher, D. E. (2006). Matrix elasticity directs stem cell lineage specification. *Cell, 126*, 677–689.

Feyissa, Z., Edossa, G. D., Gupta, N. K., & Negera, D. (2023). Development of double crosslinked sodium alginate/chitosan based hydrogels for controlled release of metronidazole and its antibacterial activity. *Heliyon, 9*, Article e20144.

García-Torres, J., Colombi, S., Macor, L. P., & Alemán, C. (2022). Multitasking smart hydrogels based on the combination of alginate and poly(3,4-ethylenedioxythiophene) properties: A review. *International Journal of Biological Macromolecules, 219*, 312–332.

Giaretta, J. E., Duan, H., Oveissi, F., Farajikhah, S., Dehghani, F., & Naficy, S. (2022). Flexible sensors for hydrogen peroxide detection: A critical review. *ACS Applied Materials & Interfaces, 14*, 20491–20505.

Grant, G. T., Morris, E. R., Rees, D. A., Smith, P. J. C., & Thom, D. (1973). Biological interactions between polysaccharides and divalent cations: The egg-box model. *FEBS Letters, 32*, 195–198.

Grijalvo, S., Nieto-Díaz, M., Maza, R. M., Eritja, R., & Díaz, D. D. (2019). Alginate hydrogels as scaffolds and delivery systems to repair the damaged spinal cord. *Biotechnology Journal, 14*, Article 1900275.

Guo, X., Wang, Y., Qin, Y., Shen, P., & Peng, Q. (2020). Structures, properties and application of alginic acid: A review. *International Journal of Biological Macromolecules, 162*, 618–628.

Gupta, K. C., & Jabrail, F. H. (2006). Glutaraldehyde and glyoxal cross-linked chitosan microspheres for controlled delivery of centchroman. *Carbohydrate Research, 341*, 744–756.

He, H., Zhang, L., Guan, X., Cheng, H., Liu, X., Yu, S., … Ouyang, J. (2019). Biocompatible conductive polymers with high conductivity and high stretchability. *ACS Applied Materials & Interfaces, 11*, 26185–26193.

Hoenig, E., Leicht, U., Winkler, T., Mielke, G., Beck, K., Peters, F., … Morlock, M. M. (2013). Mechanical properties of native and tissue-engineered cartilage depend on carrier permeability: A bioreactor study. *Tissue Engineering Part A, 19*, 1534–1542.

Huamani-Palomino, R. G., Córdova, B. M., Pichilingue, L. E. R., Venâncio, T., & Valderrama, A. C. (2021). Functionalization of an alginate-based material by oxidation and reductive amination. *Polymers, 13*, 255.

Ionita, G., Ariciu, A. M., Smith, D. K., & Chechik, V. (2015). Ion exchange in alginate gels-dynamic behavior revealed by electron paramagnetic resonance. *Soft Matter, 11*, 8968–8974.

Işıklan, N., Kurşun, F., & İnal, M. (2010). Graft copolymerization of itaconic acid onto sodium alginate using benzoyl peroxide. *Carbohyd. Polym., 79*, 665–672.

Ji, D., Park, J. M., Oh, M. S., Nguyen, T. L., Shin, H., Kim, J. S., … Kim, J. (2022). Superstrong, superstiff, and conductive alginate hydrogels. *Nature Communications, 31*, 3019.

Joddar, B., Garcia, E., Casas, A., & Stewart, C. M. (2016). Development of functionalized multi-walled carbon-nanotube-based alginate hydrogels for enabling biomimetic technologies. *Scientific Reports, 6*, Article 32456.

Kaklamani, G., Kazaryan, D., Bowen, J., Iacovella, F., Anastasiadis, S. H., & Deligeorgis, G. (2018). On the electrical conductivity of alginate hydrogels. *Regen. Biomater., 5*, 293–301.

Klein, M., & Poverenov, E. (2020). Natural biopolymer-based hydrogels for use in food and agriculture. *Journal of the Science of Food and Agriculture, 100*, 2337–2347.

Kumar, A., & Kumar, A. (2017). Development and characterization of tripolymeric and bipolymeric composite films using glyoxal as a potent crosslinker for biomedical application. *Materials Science and Engineering: C, 73*, 333–339.

Lee, B. H., Li, B., & Guelcher, S. A. (2021). Gel microstructure regulates proliferation and differentiation of MC3T3-E1 cells encapsulated in alginate beads. *Acta Biomaterialia, 8*, 1693–1702.

LeRoux, M. A., Guilak, F., & Setton, L. A. (1999). Compressive and shear properties of alginate gel: Effects of sodium ions and alginate concentration. *Journal of Biomedical Materials Research, 47*, 46–53.

Li, Z. J., Srebnik, S., & Rojas, O. J. (2022). Competing effects of hydration and cation complexation in single-chain alginate. *Biomacromolecules, 23*, 1949–1957.

Luu, C. H., Nguyen, G., Le, T. T., Nguyen, T. N., Phan, V. H. G., Murugesan, M., … Thambi, T. (2022). Graphene oxide-reinforced alginate hydrogel for controlled release of local anesthetics: Synthesis, characterization, and release studies. *Gels, 16*, 246.

Manzoor, A., Dar, A. H., Pandey, V. K., Shams, R., Khan, S., Panesar, P. S., … Khan, S. A. (2022). Recent insights into polysaccharide-based hydrogels and their potential applications in food sector: A review. *International Journal of Biological Macromolecules, 213*, 987–1006.

Meng, H., Xiao, P., Gu, J., Wen, X., Xu, J., Zhao, C., … Chen, T. (2014). Self-healable macro−/microscopic shape memory hydrogels based on supramolecular interactions. *Chemical Communications, 50*, 12277–12280.

Miyata, T., Kurokawa, K., & De Strihou, C. V. (2000). Advanced glycation and lipoxidation end products: Role of reactive carbonyl compounds generated during carbohydrate and lipid metabolism. *J. Am. Soc. Nephrol., 11*, 1744–1752.

Mottet, L., Le Cornec, D., Noël, J.-M., Kanoufi, F., Delord, B., Poulin, P., & Bremond, J. B. N. (2018). A conductive hydrogel based on alginate and carbon nanotubes for probing microbial electroactivity. *Soft Matter, 14*, 1434–1441.

Murugan, P., Nagarajan, R. D., Sundramoorthy, A. K., Ganapathy, D., Atchudan, R., Nallaswamy, D., & Khosla, A. (2022). Electrochemical detection of H_2O_2 using an activated glassy carbon electrode. *ECS Sensors Plus, 1*, Article 034401.

Panigrahi, D., Kumar, S., & Dhar, A. (2019). Modulating chain conformations of polyvinyl alcohol through low cost and nontoxic glyoxal crosslinker: Application in high performance organic transistors. *Organic Electronics, 65*, 193–200.

Pérez-Madrigal, M. M., Torras, J., Casanovas, J., Häring, M., Alemán, C., & Díaz Díaz, D. (2017). Paradigm shift for preparing versatile M^{2+}-free gels from unmodified sodium alginate. *Biomacromolecules, 18*, 2967–2979.

Pragya, A., Mutalik, S., Younas, M. W., Pang, S.-K., So, P.-K., Wang, F., … Noor, N. (2021). Dynamic cross-linking of an alginate–acrylamide tough hydrogel system: Time-resolved in situ mapping of gel self-assembly. *RSC Advances, 11*, 10710–10726.

Puiggalí-Jou, A., Babeli, I., Roa, J. J., Zoppe, J. O., Garcia-Amorós, J., Ginebra, M.-P., … García-Torres, J. (2021). Remote spatiotemporal control of a magnetic and electroconductive hydrogel network via magnetic fields for soft electronic applications. *ACS Applied Materials & Interfaces, 13*, 42486–42501.

Puiggalí-Jou, A., Cazorla, E., Ruano, G., Babeli, I., Ginebra, M. P., García-Torres, J., & Alemán, C. (2020). Electroresponsive alginate-based hydrogels for controlled release of hydrophobic drugs. *ACS Biomat. Sci. Eng., 6*, 6228–6240.

Quero, F., Nogi, M., Lee, K.-Y., Vanden Poel, G., Bismarck, A., Mantalaris, A., … Eichhorn, S. J. (2011). Cross-linked bacterial cellulose networks using glyoxalization. *ACS Applied Materials & Interfaces, 3*, 490–499.

Rajaram, A., Schreyer, D. J., & Chen, D. X. (2015). Use of the polycation polyethyleneimine to improve the physical properties of alginate-hyaluronic acid hydrogel during fabrication of tissue repair scaffolds. *J. Biomater. Sci. Polym. Ed., 26*, 433–445.

Ramires, E. C., Megiatto, J. D., Jr., Gardrat, C., Castellan, A., & Frollini, E. (2010). Biobased composites from glyoxal-phenol matrices reinforced with microcrystalline cellulose. *Polimeros, 20*, 126–133.

Ren, K., Cheng, Y., Huang, C., Chen, R., Wang, Z., & Wei, J. (2019). Self-healing conductive hydrogels based on alginate, gelatin and polypyrrole serve as a repairable circuit and a mechanical sensor. *Journal of Materials Chemistry B, 7*, 5704–5712.

Rojas, J., & Azevedo, E. (2011). Functionalization and crosslinking of microcrystalline cellulose in aqueous media: A safe and economic approach. *Int. J. Pharm. Sci. Rev. Res., 8*, 28–36.

Samorezov, J. E., Morlock, C. M., & Alsberg, E. (2015). Dual ionic and photo-crosslinked alginate hydrogels for micropatterned spatial control of material properties and cell behavior. *Bioconjugate Chemistry, 26*, 1339–1347.

Schwartz, M. P., Fairbanks, B. D., Rogers, R. E., Rangarajan, R., Zaman, M. H., & Anseth, K. S. (2010). A synthetic strategy for mimicking the extracellular matrix provides new insight about tumor cell migration. *Integrative Biology, 2*, 32–40.

Siboro, S. A. P., Anugrah, D. S. B., Ramesh, K., Park, S.-H., Kim, H.-R., & Lim, K. T. (2021). Tunable porosity of covalently crosslinked alginate-based hydrogels and its significance in drug release behavior. *Carbohydrate Polymers, 260*, Article 117779.

Solberg, A., Draget, K. I., Schatz, C., & Christensen, B. E. (2023). Alginate blocks and block polysaccharides: A review. *Macromolecular Symposia, 408*, Article 2200072.

Szabó, L., Gonelle-Gispert, C., Montanari, E., Noverraz, F., Bornet, A., Bühler, L. H., & Gerber-Lemaire, S. (2019). Cross-reactive alginate derivatives for the production of dual ionic–covalent hydrogel microspheres presenting tunable properties for cell microencapsulation. *ACS Applied Polymer Materials, 1*, 1326–1333.

Teepoo, S., Dawan, P., & Barnthip, N. (2017). Ultrasensitive label-free sensing of il-6 based on pase functionalized carbon nanotube micro-arrays with rna-aptamers as molecular recognition elements. *Biosensors, 7*, 47.

Volpi, M., Paradiso, A., Costantini, M., & Święszkowski, W. (2022). Hydrogel-based fiber biofabrication techniques for skeletal muscle tissue engineering. *ACS Biomat. Sci. Eng., 8*, 379–405.

Wan, J., Wang, W., Yin, G., & Ma, X. (2012). Nonenzymatic H_2O_2 sensor based on Pt nanoflower electrode. *Journal of Cluster Science, 2012*(23), 1061.

Wang, J., Liu, S., Huang, J., Ren, K., Zhu, Y., & Yang, S. (2023). Alginate: Microbial production, functionalization, and biomedical applications. *International Journal of Biological Macromolecules, 242*, Article 125048.

Wang, L., Shansky, J., Borselli, C., Mooney, D., & Vandenburgh, H. (2012). Design and fabrication of a biodegradable, covalently crosslinked shape-memory alginate scaffold for cell and growth factor delivery. *Tissue Engineering. Part A, 19-20*, 2000–2007.

Wang, Z., & Liu, R. (2023). PEDOT:PSS-based electrochromic materials for flexible and stretchable devices. *Materials Today Electronics, 4*, Article 100036.

Yang, S., Jang, L., Kim, S., Yang, J., Yang, K., Cho, S.-W., & Lee, J. Y. (2016). Polypyrrole/alginate hybrid hydrogels: Electrically conductive and soft biomaterials for human mesenchymal stem cell culture and potential neural tissue engineering applications. *Macromolecular Bioscience, 16*, 1653–1661.

Yang, Y., Xu, L., Wang, J., Meng, Q., Zhong, S., Gao, Y., & Cui, X. (2022). Recent advances in polysaccharide-based self-healing hydrogels for biomedical applications. *Carbohydrate Polymers, 283*, Article 119161.

Zhang, J., Zhu, Y., Song, J., Yang, J., Pan, C., Xu, T., & Zhang, L. (2018). Novel balanced charged alginate/pei polyelectrolyte hydrogel that resists foreign-body reaction. *ACS Applied Materials & Interfaces, 10*, 6879–6886.